Analytical Coverage Probability Framework and Spectrum Sharing Prohibition Zone in Heterogeneous Cellular Networks with Sectored-FFR

Sani Umar Abdullahi, Jian Liu, and Seyed Alireza Mohadeskasaei
School of Computer and Communications Engineering, University of Science and Technology Beijing, Beijing 102208, P.R. China
Email: saniumar.a.ng@ieee.org; liujian@ustb.edu.cn; alireza_kasaee@yahoo.com

Abstract —In this work, an analytical coverage probability framework is derived for all the User Equipment (UE) types in a Fractional Frequency Reuse (FFR)-aided heterogeneous network leveraging tools of stochastic geometry. This framework is used to determine the minimum distance for edge femtocells to safely reuse same spectrum resources utilized by center macro users (MUEs) for successful signal transmission and decoding. A spectrum sharing prohibition zone is thus created in which only orthogonal spectrum usage is allowed between the two tiers to avoid violating the system outage constraint, and is found to be sensitive to macrocell antenna azimuth and other key network parameters. Using the macrocell center radius, R_m and the derived co-channel femtocells distance, $r_{co-F_{\min}}$, a new spatial partitioning threshold, R_f is obtained for the femtocell network, extending the spectrum sharing prohibition zone for further interference reduction. Analytical and numerical results show that the introduction of R_f and use of extended co-channel prohibition zone offers improved protection to UEs against severe cross-tier interference with enhanced throughput performance, compared to most schemes employing a single spatial partitioning parameter. The proposed scheme therefore provides guidelines for efficient deployment of closed-access femtocells with hybrid spectrum usage in multi-tier networks for lower power consumption and improved throughput performance.

Index Terms—Heterogeneous network, fractional frequency reuse, stochastic geometry, coverage probability, spectrum sharing, prohibition zone

I. Introduction

Femtocells are the lowest in hierarchy of small cells that are deployed in modern cellular networks over traditional macrocells to improve spectral efficiency and indoor coverage, while also off-loading data traffic from congested macro cells in a cost-effective manner. Femto base stations, referred to as Home eNBs (HeNBs) in LTE-Advanced nomenclature, are short range (10-30m), low-power (10-100mw), relatively inexpensive plug-and-play type access points deployed in an unplanned manner by end-users, and connected to operators' core network via broadband internet backhaul connections [1]. As they utilize licensed spectrum of the mobile network operators, femtocells are usually deployed in co-channel mode to the underlying macro base stations (MeNBs) for higher spectral efficiency, albeit at the cost of increased interference [2], but could also be deployed in dedicated spectrum for cross-tier interference avoidance, but at the cost of less spectrum utilization [3]. For security, economic reasons and backhaul limitations, many femtocells allow access to only authorized subscribers which are said to belong to a Closed Subscriber Group (CSG), barring any other User Equipments (UEs) irrespective of location or tier association. In such scenarios, inter-tier interference could severely degrade UE performance, especially when the randomly deployed femtocells are in very close proximity to high-powered macrocells [4], or for macro UEs (MUEs) located indoors within coverage range of closed-access femtocells [5]. An attractive Inter-Cell Interference Coordination (ICIC) technique well suited to current Orthogonal Frequency Division Multiple Access (OFDMA) networks to mitigate against Co-Channel Interference (CCI) in multi-tier networks is the Fractional Frequency Reuse (FFR) scheme, due to its low complexity, minimal signaling overhead, and significant coverage improvement [6]-[10]. The use of FFR is a natural trade-off between full-frequency reuse systems and systems with higher frequency re-reuse factors, by employing spectral reuse only for the edge UEs to improve their coverage, while serving cell-center UEs with full frequency for highest, possible spectral efficiency.

Investigation into the dead-spot problem for co-channel femtocells deployed very close to macrocells has gathered considerable interest in the research community [4], [11]-[14]. In [4], an Interference Limited Coverage Area (ILCA) for femtocells was derived where co-channel transmission by femtocells is avoided for a single-macrocell/single-femtocell system using a path-loss only channel model. Authors in [11] improved on this to propose a hybrid femtocell spectrum arrangement by using femto user classification based on the achievable throughput of the two LTE tiers instead of the coverage of femto cells, but do not particularly improve the edge macro user performance. Wu et al. derived in [12] an

Manuscript received January 25, 2017; revised March 28, 2017.
This work was supported by the National Major Project under Grant No. 2015ZX03001013-002.
Corresponding author email: saniumar.a.ng@ieee.org.
doi:10.12720/jcm.12.3.152-163

analytical expression for the minimum distance that co-channel femtocells can be deployed away from a MeNB as a function of azimuth angle for a 3-sector, hierarchical grid structure, and proposed a downlink power control for femtocells to prevent them transmitting when very close to the embedding macrocell. In [13], two possible Femto Exclusion Regions (FERs) are derived for co-channel operation of femtocells in an FFR-aided, two-tier, OFDMA network employing an omni-directional antenna, and ignoring other macrocells' interference in the analytical evaluation. Authors in [14] derive an optimal exclusion region centered on each femtocell to reduce cross-tier interference and minimize system power consumption, also considering a single macrocell for the entire analysis.

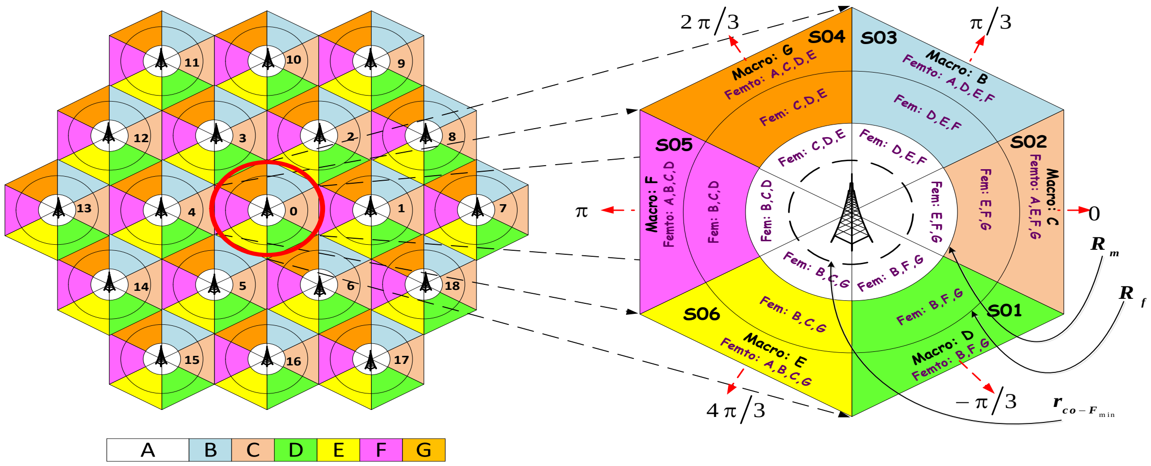

(a) (b)

Fig. 1. (a) Base station topology (b) Macrocell structure showing main-beam pointing direction of each sector.

$$M_k = \begin{cases} \sqrt{3}R_C \cos\left((k-1)\frac{\pi}{3}\right),\ \sqrt{3}R_C \sin\left((k-1)\frac{\pi}{3}\right), & k = 1:6 \ \text{ first layer} \\ 2\sqrt{3}R_C \cos\left((k-1)\frac{\pi}{6}\right),\ 2\sqrt{3}R_C \sin\left((k-1)\frac{\pi}{6}\right), & k = 7:18 \ \text{second layer} \end{cases} \tag{1}$$

In this work, we first derive analytical expressions for the coverage probability for all UE types, employing FFR overlaid with closed-access femtocells, and then use the results to define the minimum distance for co-channel operation of the edge femtocells with the underlaying FFR macrocells without violating outage constraints. Differently than [8]-[14] however, we proceed to show that extending the co-channel prohibition zone by use of a different parameter, R_f, for partitioning the femto network yields higher performance gains than previous works. The effects of both inter-tier and intra-tier interference are well investigated in this work, including at the boundary of cell-center and cell-edge regions, which is commonly ignored in most prior works. The proposed analytical framework provides insights into the relationship between different network parameters and key performance metrics for hybrid mode operation of femtocells overlaid in FFR-aided macrocell networks.

The structure of the paper is as follows: Section II presents the system model. In Section III, the analytical framework for obtaining the coverage probability for the different kinds of UEs based on their spatial locations within the cell area is derived, while Section IV analyses the co-channel prohibition zone and spatial partitioning thresholds. Section V shows performance evaluation and simulation results and finally, the work is concluded in Section VI.

II. System Model

A. Topology

The focus is on downlink of an OFDMA two-tier network using FFR where the macrocells are deployed after careful design and planning as regular tessellations of hexagonally-shaped coverage areas with the macro base stations (MeNBs) located at the center of the hexagons, while closed-access femtocells, each with radius R_{HeNB} are distributed over the entire cellular network in indoor environments according to a spatial Poisson Point Process (PPP) denoted by Ω_f with intensity λ_f.

The entire network is made up of 19 macrocells in total, with the macrocell of interest M_0, located at the origin (0, 0) of the R^2 plane with coverage area $|C|$, surrounded by 2 layers of neighbouring macrocells, where M_k, represents the macrocell as shown in Fig. 1(a). The first layer consists of six macrocells labeled (1-6) with the locations M_k at (x_k, y_k), while the second layer consists of 12 macrocells (labeled 7-18) with the locations of M_k at macrocells (labeled 7-18) with the locations of M_k at (p_k, q_k) as given in (1) respectively. The inter-site distance is given by $\sqrt{3}R_C$, with R_C as the cell radius.

For analytical convenience, M_0 is approximated as a disc which has the same area as the respective hexagon given as $|C| = \pi R_C^{\,2}$ as shown in Fig. 1. The radius of the circular cell is defined as $R_C = R_{Hex}\sqrt{\frac{3\sqrt{3}}{2\pi}}$ where R_{Hex} is the radius of the original hexagon. Each macrocell contains six equal sectors: $S_{k1}, S_{k2} ......S_{k6}$ where the bore-sight of each sector, $S_{kl}\,(l \in \{1,2,3,4,5,6\})$, is given by $\check{\Upsilon}_l = 2(l-2)\frac{\pi}{6}$ such that the arrangement of the sectors is as shown in Fig. 1(b). The average number of femtocells per macrocell is therefore given as $N_f = \lambda_f\,|C|$. Due to the symmetric structure of the macrocell sectors, we hereby present the analytical evaluation for one sector only (sector S_{03}) for brevity, since similar results will be realized for other sectors. For each MeNB sector, the horizontal antenna gain pattern is given by;

$$G_m(\Upsilon) = G_m^{(\max)} - \min\left\{12\left(\frac{\Upsilon}{HPBW}\right), A_m\right\} \qquad (2)$$

where $-180^{\circ} \le \Upsilon \le 180^{\circ}$ is the azimuth angle relative to the main-lobe, $A_m = 25$ dB is the maximum attenuation and for a six-sectored antenna $HPBW = 35°$ [15]. The azimuth angle of a UE at (r,θ) relative to the main beam pointing direction of sector $S_{0l}\,(l \in \{1,2,3,4,5,6\})$ is given by $\Upsilon = \theta - \check{\Upsilon}_l$, while the azimuth angle of a UE at (r,θ) with respect to the main beam pointing direction of sector $S_{kl}\,(\mathrm{k} \in \{1,2,3,4....18\},\ l \in \{1,2,3,4.,5,6\})$ is a function of r and θ given by;

$$\Upsilon_{kl} = \begin{cases} \operatorname{atan2}\left(\dfrac{r\sin\theta - y_k}{r\cos\theta - x_k}\right) - \check{\Upsilon}_l & k = 1:6 \\ \operatorname{atan2}\left(\dfrac{r\sin\theta - q_k}{r\cos\theta - p_k}\right) - \check{\Upsilon}_l & k = 7:18 \end{cases} \qquad (3)$$

B. SINR and Interference Analysis

The downlink wireless channel model is comprised of path-loss with exponent α, and small scale fading, G_Z, between any interfering base station, ψ, and the UE, u, in consideration which is i.i.d (independent and identically distributed) exponentially distributed with mean μ (corresponding to Rayleigh fading). Wall-penetration loss, ϑ, is considered for indoor-outdoor transmissions, while a double wall- penetration loss ϑ^2, is considered for indoor transmissions from one femto-cell to neighbouring indoor femto-cells/UEs. The instantaneous SINR of a UE u in the reference cell M_0 on sub-carrier k of resource block n at a random distance from M_0 is given in (4);

$$SINR_u^{n_k} = \frac{P_{M_{0l,u}}\, g_u r^{-\alpha}}{\sigma^2 + \sum\limits_{\psi\in\psi_m} P_{M_{k,l}} G_\psi R_\psi^{-\alpha} + \sum\limits_{\psi\in\psi_f} P_F G_\psi R_\psi^{-\alpha}} \qquad (4)$$

In (4), r represents the distance of the UE from M_0, $P_{M_{kl,u}} = G_M(\Upsilon_{kl})G_u P_{M_{kl,Tx}}$ where $G_M(\Upsilon_{kl})$ is the antenna gain of sector S_{kl} along Υ_{kl}, G_u is the UE antenna gain, $P_{M_{kl,Tx}}$ is the transmit power per resource block of sector S_{kl}. g_u is the exponentially distributed channel power gain (Rayleigh fading), σ^2 represents additive noise power, while the second and third denominator terms represent the interference from macrocells (I_M) and femtocells (I_{FM}) respectively. $P_F = G_F G_u P_{F,Tx}$ where G_F is HeNB antenna gain, G_u is as earlier defined, $P_{F,Tx}$ is the serving HeNB transmit power per resource block. x represents set of interfering macrocells (x=m) and femtocells (x=f) respectively, which depend on the location and type of UE under consideration. Taking sector S_{03} as reference for brevity, Table I defines some important sets of macro base stations, including the interfering sets in each case, which is key in the SINR distribution framework to be developed. Interference to/from all sectors is duly considered in the simulation.

TABLE I: NOTABLE SETS OF MACROCELLS FOR INTERFERENCE ANALYSIS TO SECTOR S03 OF CELL M0

Set	Cell ID's	Description of Set
C_a	{0 -18}	Set of all macrocells in the system
C_o	{1-18}	All macrocells that use sub-band A (CR spectrum) and will interfere with a UE in CR of M_o
C_1	{5, 14, 15, 16}	Macrocells on sub-band B causing interference in S_{03} of M_o
C_2	{NIL}	Macrocells that use sub-band C and will cause interference in S_{03} of M_o
C_3	{3, 10, 11}	Macrocells on sub-band D causing interference in S_{03} of M_o
C_4	{2, 9}	Macrocells that use sub-band E and will cause interference in S_{03} of M_o
C_5	{1, 7, 8}	Macrocells on sub-band F and will cause interference in S_{03} of M_o
C_6	{NIL}	Macrocells that use sub-band G and will cause interference in S_{03} of M_o

The set of femtocells that will interfere with a UE (whether macro or femto) in a given region will be those femtocells that share same spectrum with the specified UE in the same area. Since the femtocells are distributed according to a spatial PPP, the set of interfering femtocells will form a marked Spatial PPP which is a subset of initial PPP Ω_f, since the independent thinning of a PPP leads to another PPP [16], [17], thereby retaining the randomness of the femtocell distribution. Table II shows the interfering femtocell analysis where the total femtocell density is weakened in each case either by probability of interfering femtocell being in same region with intended UE, probability of accessing same sub-band as intended UE in same region, or both. In Table II,

$\mathcal{F}_{\mathcal{S}}$ denotes the number of resource blocks in sub-band $\mathcal{S}$, with A representing center region (CR) resources and ER representing edge resources respectively, q_x represents the density thinning factor for interfering femtocells to UE *x*, $p_{f-S_1 \cup S_2 \cup S_3 \cup S_4 \cup S_5}$ is the probability of femtocell being in any of the listed sets and utilizing sub-bands D, E and/or F.

TABLE II: INTERFERING MACROCELLS AND FEMTOCELLS TO ALL UE TYPES IN SECTOR S03 OF CELL M0

Type of User	Sets of Interfering Macrocells ψ_m	Description of interfering femtocells	Thinned density of interfering femtocells
CR MUE	C_o	All Edge femtocells using sub-band A	$q_{mc}\lambda_f$ such that $0 \le q_{mc} \le 1$ $q_{mc} = \frac{\text{Edge Area}}{\text{Macrocell coverage Area}} * \frac{\mathcal{F}_A}{\mathcal{F}_{ER}}$
ER MUE	C_1	All femtocells using sub-band B. i.e. In S_{01}, S_{05}, and S_{06}	$q_{ef}\lambda_f$ such that $0 \le q_{ef}\lambda_f \le 1$ $q_{ef} = 0.5$
CR FUE	$C_3 U\ C_4 U\ C_5$	All femtocells using D, E, F. i.e. In S_{01}, S_{02}, S_{03}, S_{04}, and S_{05}	$q_{fc}\lambda_f$ such that $0 \le q_{fc} \le 1$ $q_{fc} = p_{f-S_1 \cup S_2 \cup S_3 \cup S_4 \cup S_5}$
ER FUE	$\left(\frac{\mathcal{F}_A}{\mathcal{F}_{(A+D+E+F)}} * C_a\right) + \left(\frac{\mathcal{F}_{(D+E+F)}}{\mathcal{F}_{(A+D+E+F)}} * C_3 \cup C_4 \cup C_5\right)$	ER Femtocells using sub-band A and/or ER Femtocells using D,E,F	$\lambda_{FF} = \left(\frac{\mathcal{F}_A}{\mathcal{F}_{(A+D+E+F)}} * q_{mc}\lambda_f\right) + \left(\frac{\mathcal{F}_{(D+E+F)}}{\mathcal{F}_{(A+D+E+F)}} * q_{fc}\lambda_f\right)$

$$CP_{mc} = \frac{2}{R_m{}^2 - R_0{}^2} \int_{R_0}^{R_m} \exp\left(-\frac{\mu\gamma r^\alpha \sigma^2}{P_{M_{0l}}}\right) \left(\sum_{i \in \psi_m} \frac{1}{1+\gamma\left(\frac{r}{\|r-b_i\|}\right)^\alpha} \right) \times \exp\left(-\frac{2\pi^2 q_{mc}\lambda_f \cdot \left(\mu\gamma r^\alpha \vartheta \frac{P_f}{P_m}\right)^{\frac{2}{\alpha}}}{\alpha \sin\left(\frac{2\pi}{\alpha}\right)} \right) r dr \tag{5}$$

III. PER-USER COVERAGE PROBABILITY

The coverage probability of a UE *x* on RB *n* is defined as the probability that the UE's instantaneous SINR level exceeds a certain threshold γ, which is conditioned on the locations of the MUE/FUE and the serving and interfering base stations. Mathematically, it is equivalent to the Complementary Cumulative Distribution Function (CCDF) of the SINR distribution and is expressed as $CP_x = \Pr(SINR_x^{n_k} > \gamma)$. As earlier sated, the analytical framework derived here is with respect to sector S_{03} of cell M_0 for brevity.

A. Theorem 1

The coverage probability of a center MUE based on the proposed model averaged over the center region is approximated as in (5).

Proof: Based on uniform user distribution in the CR and since UEs are defined by distance and angle in polar coordinates, the coverage probability averaged over the center area is expressed as in (6) where R_H and R_L are the upper and lower radii of the circumference defining the region where the reference UE is located.

$$\left(CP_{mc} \mid r,\theta\right) = \int_0^{2\pi}\int_{R_L}^{R_H} \mathrm{P}\left(SINR > \gamma \mid r,\theta\right) f_r(r) f_\theta(\theta) dr d\theta \tag{6}$$

$$f_{r,mue}(r) = \begin{cases} \frac{2r}{R_m^2 - R_o^2}, & R_0 \le r \le R_m \quad \text{(CR)} \\ \frac{2r}{R_C^2 - R_m^2}, & R_m \le r \le R_C \quad \text{(ER)} \end{cases} \tag{7}$$

$$f_{\theta,mue}(r) = \begin{cases} \frac{1}{2\pi}, & 0 \le \theta \le 2\pi \quad \text{(CR)} \\ \frac{1}{\pi/3}, & \theta_L \le \theta \le \theta_H \quad \text{(ER)} \end{cases} \tag{8}$$

where $f_r(r)$ and $f_\theta(\theta)$ are the Probability Density Function (PDF) of the user location defined by distance, *r*, and angular position, θ. R_0 is the minimum distance of a UE from serving base station (25m in this work), R_m and R_C are as earlier defined, θ_L and θ_H are the lower and upper angle limits of the region surrounding the considered UE ($\pi/6$ and $\pi/2$ respectively for the sector S_{03} of cell M_0 in consideration). Since an omnidirectional antenna is used in CR, the interference performance for CR MUEs will have isotropic performance and the instantaneous SINR will vary very little with polar angle as shown in [18]. Hence, (6) can be re-written as $CP_{mc} \mid r$, and considering Rayleigh fading ($g_m = \exp(\mu)$), is given as;

$$CP_{mc} = \frac{2}{R_m^2 - R_0^2} \int_{R_0}^{R_m} \mathrm{P}\left(SINR > \gamma \mid r\right) r dr \tag{9}$$

where the conditional CCDF (i.e. the integral term) can be written as;

$$\mathrm{P}\left(SINR > \gamma \mid r\right) = \mathrm{E}_{I_M, I_{FM}}\left[\mathrm{P}\left[-\mu\left(\sigma^2 + I_M + I_{FM}\right)\frac{\gamma r^{\alpha}}{P_m}\right]\right] \tag{10}$$

Upon further simplification;

$$\mathrm{P}[SINR > \gamma] = e^{-\frac{\mu\gamma r^{\alpha}\sigma^2}{P_m}}\mathcal{L}_{I_M}\left(\frac{\mu\gamma r^{\alpha}}{P_m}\right)\mathcal{L}_{I_{FM}}\left(\frac{\mu\gamma r^{\alpha}}{P_m}\right) \tag{11}$$

where $\mathcal{L}_{I_M}(s)$ and $\mathcal{L}_{I_{FM}}(s)$ represent the Laplace transforms of the random variables I_M and I_{FM} respectively, evaluated at $s\left(s = (\mu\gamma r^{\alpha})/P_m\right)$. Substituting (11) into (9);

$$CP_{mc} = \frac{2}{R_m^2 - R_0^2}\int_{R_0}^{R_m} e^{-\frac{\mu\gamma r^{\alpha}\sigma^2}{P_m}}\mathcal{L}_{I_M}\left(\frac{\mu\gamma r^{\alpha}}{P_m}\right)\mathcal{L}_{I_{FM}}\left(\frac{\mu\gamma r^{\alpha}}{P_m}\right) r dr \tag{12}$$

From (4), I_M is a weighted sum of independent exponential random variables, and hence $\mathcal{L}_{I_M}$ can be represented by the moment generating function (MGF) of exponential distribution [19].

$$\mathcal{L}_{I_M} = \sum_{i\in\psi_m}\frac{\mu}{\mu + \frac{\mu\gamma r^{\alpha}}{P_m}P_i R_i^{-\alpha}} = \sum_{i\in\psi_m}\frac{1}{1+\gamma\left(r/\left\|r-b_i\right\|\right)^{\alpha}} \tag{13}$$

Since $P_m = P_i = P$ for all macro base stations, and $R_i = r - b_i$, where r is the distance vector from the center cell M_0 to the UE under consideration and b_i represents the distance vector from M_0 to the interfering macrocell M_i. The femto interference I_{FM} follows a shot noise process [16], [17], hence its Laplace transform is given below;

$$\mathcal{L}_{I_{FM}}(s) = E_{G_i,\psi_f}\left[\exp - s\left(\sum_{i\in\psi_f} P_F \vartheta G_i R_i^{-\alpha}\right)\right] \tag{14}$$

$$\mathcal{L}_{I_{FM}}(s) = \mathrm{E}_{\psi_f}\left(\prod_{i\in\psi_f}\mathcal{L}_g\left(sR_i^{-\alpha}\vartheta P_f\right)\right) \tag{15}$$

With change of notation and from Probability Generating Functional (PGFL) of the PPP,

$$\mathcal{L}_{I_{FM}}(s) = \exp\left(-2\pi q_{me}\lambda_f\int_r^{\infty}\left(1-\mathcal{L}_g\left(sx^{-\alpha}\vartheta P_f\right)\right)x dx\right) \tag{16}$$

After change of integration order and substituting for $\mathcal{L}_g\left(sx^{-\alpha}\vartheta P_f\right)$;

$$\mathcal{L}_{I_{FM}}(s) = \exp\left(-2\pi q_{me}\lambda_f \underbrace{\int_0^{\infty}\int_r^{\infty}\left(1-e^{-sx^{-\alpha}\vartheta P_f g}\right) f(g) x\, \mathrm{d}x\mathrm{d}g}_{(Y)}\right) \tag{17}$$

After integration by parts and using the Gamma function properties;

$$Y = \frac{1}{2}\left(s\vartheta P_f\right)^{\frac{2}{\alpha}}\Gamma\left(1-\frac{2}{\alpha}\right)\mathrm{E}_g\left(g^{\frac{2}{\alpha}}\right) \tag{18}$$

Substituting for Y and using $\mathrm{E}_g\left(g^{2/\alpha}\right) = \Gamma\left(\frac{2+\alpha}{\alpha}\right)$ and $\Gamma\left(1-\frac{2}{\alpha}\right)\Gamma\left(\frac{2+\alpha}{\alpha}\right) = \frac{2\pi}{\alpha\sin(2\pi/\alpha)}$ [20], for $\alpha > 2$;

$$\mathcal{L}_{I_{FM}}(s) = \exp\left(-\pi q_{me}\lambda_f\left(\mu\gamma r^{\alpha}\vartheta\frac{P_f}{P_m}\right)^{\frac{2}{\alpha}}\frac{2\pi}{\alpha\sin(2\pi/\alpha)}\right) \tag{19}$$

Replacing $\mathcal{L}_{I_M}(s)$ and $\mathcal{L}_{I_{FM}}(s)$ in (12) gives the result.

B. *Theorem 2*

The coverage probability of an ER MUE averaged over sector S_{03} of M_0 is approximated as in (20). The respective sets of interfering macrocells and femto densities are used according to Table II. Angular position of sector S_{03} of M_0 is also considered for ER analysis, while the rest of the proof is similar to Theorem 1.

C. *Theorem 3*

The coverage probability of center FUEs as defined in the proposed model is given in (21), where r_{fue} is the distance vector from an FUE to its serving HeNB, R_{HeNB} is the radius of the serving HeNB, r is the distance vector of the tagged HeNB (and not the FUE) to macrocell M_0 for the worst case interference scenario.

Proof: For FUE coverage analysis, both the PDF of FUE location in its femtocell and that of the serving femtocell in the respective macrocell are considered. For emphasis, expectation over angular position of S_{03} in M_0 is also included and double-wall penetration loss, ϑ^2 to represent femto-to-femto interference. The rest of the proof is same as Theorem 1.

$$CP_{me} = \frac{1}{\pi/3}\cdot\frac{2}{R_C^{\,2} - R_m^{\,2}}\int_{R_m}^{R_C}\int_{\pi/6}^{\pi/2}\exp\left(-\frac{\mu\gamma r^{\alpha}\sigma^2}{P_{M_{01}}}\right)\left(\sum_{i\in\psi_m}\frac{1}{1+\gamma\left(r/\left\|r-b_i\right\|\right)^{\alpha}}\right)\exp\left(-\frac{2\pi^2 q_{me}\lambda_f\left(\mu\gamma r^{\alpha}\vartheta\left(P_f/P_m\right)\right)^{\frac{2}{\alpha}}}{\alpha\sin(2\pi/\alpha)}\right) r dr d\theta \tag{20}$$

$$CP_{fc} = \frac{1}{\pi/3} \cdot \frac{2}{R_{HeNB}^{2}} \frac{2}{R_f^{2}} \int_0^{R_{HeNB}} \int_0^{R_f} \int_{\pi/6}^{\pi/2} \exp\left(-\frac{\mu\gamma r_{fue}{}^{\alpha}\sigma^2}{P_f}\right) \left(\sum_{i \in \psi_m} \frac{1}{1+\gamma\vartheta \frac{P_m}{P_f}\left(r_{fue}/\|r-b_i\|\right)^{\alpha}} \right) \times$$
$$\exp\left(-\frac{2\pi^2 q_{fc}\lambda_f \cdot \left(\mu\gamma r^{\alpha}\vartheta \frac{P_f}{P_m}\right)^{\frac{2}{\alpha}}}{\alpha \sin\left(\frac{2\pi}{\alpha}\right)} \right) r_{fue} r dr_{HeNB} dr d\theta \tag{21}$$

$$CP_{fe} = \frac{1}{\pi/3} \cdot \frac{2}{R_{HeNB}^{2}} \frac{2}{R_C^{2} - R_f^{2}} \int_0^{R_{HeNB}} \int_{R_f}^{R_C} \int_{\pi/6}^{\pi/2} \exp\left(-\frac{\mu\gamma r_{fue}{}^{\alpha}\sigma^2}{P_f}\right) \left(\sum_{i \in \psi_m} \frac{1}{1+\gamma\vartheta \frac{P_m}{P_f}\left(r_{fue}/\|r-b_i\|\right)^{\alpha}} \right) \times$$
$$\exp\left(-\frac{2\pi^2 \lambda_{FF} \left(\mu\gamma r^{\alpha}\vartheta \frac{P_f}{P_m}\right)^{\frac{2}{\alpha}}}{\alpha \sin\left(\frac{2\pi}{\alpha}\right)} \right) r_{fue} r dr_{HeNB} dr d\theta \tag{22}$$

$$\exp\left(-\frac{\mu\gamma_F r_{fue}{}^{\alpha}\sigma^2}{P_f}\right) \left(\frac{1}{1+\gamma_F\vartheta \frac{P_m}{P_f}\left(r_{fue}/\|r-b_i\|\right)^{\alpha}} \right) \exp\left(-\frac{2\pi^2 \lambda_{FF} \left(\mu\gamma r^{\alpha}\vartheta \frac{P_f}{P_m}\right)^{\frac{2}{\alpha}}}{\alpha \sin(2\pi/\alpha)} \right) \geq 1-\varepsilon_F \tag{23}$$

$$r_{co-F_{\min}} \geq \left[r_{fue}^{\alpha} P_m \gamma_F \vartheta \left\{ P_f \left(\frac{1}{1-\varepsilon_F} \exp\left(-\frac{\mu\gamma_F r_{fue}{}^{\alpha}\sigma^2}{P_f}\right) \exp\left(-\frac{2\pi^2 \lambda_{FF} \left(\mu\gamma r^{\alpha}\vartheta \frac{P_f}{P_m}\right)^{\frac{2}{\alpha}}}{\alpha \sin\left(\frac{2\pi}{\alpha}\right)} \right) - 1 \right) \right\}^{-1} \right]^{\frac{1}{\alpha}} \tag{24}$$

D. Theorem 4

The coverage probability for an ER FUE averaged over sector S_{03} of M_0 is given in (22). The proof is same as Theorem 3, with only a change in the respective interfering macro and femtocells.

IV. Spatial Partitioning Thresholds and Co-Channel Prohibition Zone

A. Minimum Co-Channel Distance and Spectrum Sharing Prohibition Zone

For any UE x to successfully decode transmitted signals, it must satisfy some quality of service constraint, such that its outage probability does not exceed a certain threshold, $\left(\Pr\left(SINR_x \leq \gamma\right)\right) \leq \varepsilon_x$, where $0 \leq \varepsilon_x \leq 1$ denotes the maximum outage constraint in the target area. This is particularly more critical for FUEs, due to the much higher transmit powers of macrocells compared to femtocells, and when located very close to MeNBs, the outage probability of the FUE could most likely exceed ε_F leading to lack of coverage. In such scenarios, the interference from the central MeNB, M_0 would be the most significant and degrading macro interference to the FUEs, hence we consider only its effect in the analytical derivation of the minimum co-channel femto distance away from M_0 represented by $r_{co\text{-}F_{min}}$.

In the simulation, all possible interference sources are duly considered. Since the use FFR will orthogonolize macro and femto spectrum usage in the same region, our primary focus here is to derive the minimum distance that edge femtocells can share same spectrum with macrocells (sub-band A), while maintaining the quality of service constraint. This implies that the coverage probability derived for edge femtocells in (22) must satisfy the given constraint, $CP_{fe} = 1 - \varepsilon_F$. Considering the conditional CCDF only, the evaluation of the minimum co-channel distance is given in (23) by solving for r from (22). For clarity, r is replaced with $r_{co\text{-}F_{min}}$, which is the desired minimum distance derived in (24) as earlier defined. In this region, a spectrum sharing prohibition zone is thus created where FUEs must utilize orthogonal sub-bands (edge sub-bands) to the macrocell network for coverage guarantee.

The expression for $r_{co\text{-}F_{min}}$ could be further simplified for an interference limited scenario where thermal noise is negligible ($\sigma^2 = 0$) and due to double wall-penetration losses and low femto transmit powers, co-tier femto interference can also be ignored to yield the result in (25).

$$r_{co-F_{\min}} \approx \left[\frac{r_{fue}^{\alpha} P_m \gamma_F \vartheta}{P_f \left(\frac{1}{1-\varepsilon_F} - 1 \right)} \right]^{\frac{1}{\alpha}} \tag{25}$$

$r_{co\text{-}F_{min}}$ is thus found to be a function of key system parameters such as transmit powers of both macro and femtocells, the outage constraints (γ and ε_F), interfering femtocell density (λ_{FF}), path-loss exponent (α) and the wall-penetration loss (ϑ). We will show in subsequent sections that even though edge FUEs can safely reuse center region macro spectrum at this distance and has been used in other works as the center region determinant [12]-[14], it is more beneficial from a performance point of view to employ different thresholds for partitioning the macrocell and femtocell networks respectively.

B. Macro Center Region Determination

In this work, two different spatial portioning thresholds are employed, R_m and R_f, for the macrocell and femtocell networks respectively, so that the prohibition zone is extended from $r_{co\text{-}F_{min}}$ up to R_f, where co-channel operation between the two tiers is prevented for improved cross-tier interference minimization. For the macrocell network, although in reality MUEs measure received pilot signals to determine average received SINR which is used to classify cell-center and cell-edge UEs, in this section for the sake of tractability, we define a circular distance R_m, which corresponds to the point where throughput of center region and edge region MUEs are equal as the partitioning threshold of center and edge regions respectively. By so doing, a more equitable distribution of resources to both regions is guaranteed. Using the UE SINR distribution derived in (5), (20-22), we define the long-term expected throughput per sub-channel (bps/Hz) with L-discrete rates similar to [3] as thus;

$$t = \sum_{l=1}^{L-1} b_l \Pr\left[\gamma_l \le SIR < \gamma_{l+1}\right] + b_L \Pr\left[SIR \ge \gamma_L\right] \tag{26}$$

$$t_j = \sum_{l=1}^{L-1} b_l . \left(\mathrm{P}_{C_j}(\gamma_l) - \mathrm{P}_{C_j}(\gamma_{l+1}) \right) + b_L . \mathrm{P}_{C_j}(\gamma_L) \tag{27}$$

where $j \in \{M_{CR}; M_{ER}; F_{CR}; F_{ER}\}$

For simplification, we assume $b_l = l$, $\gamma_l = \Phi(2^l - 1)$ for $l = 1, ...L$. The expected throughput for all the different kinds of UEs is derived by multiplying (27) with the respective spectrum allocation factor as given in (28);

$$\begin{cases} T_{M_{CR}} = \rho t_{M_{CR}} \\ T_{M_{ER}} = (1-\rho) t_{M_{ER}} \\ T_{F_{CR}} = {(1-\rho)}/{2}\, t_{F_{CR}} \\ T_{F_{ER}} = \left(\rho + {(1-\rho)}/{2} \right) t_{F_{ER}} \end{cases} \tag{28}$$

where $\rho = |\mathcal{F}_{CR}| / |\mathcal{F}_T|$ is the ratio of resources available to CR, $\mathcal{F}_{CR}$, to total available resources $\mathcal{F}_T$. R_m is therefore defined at the point $T_{M_{CR}} = T_{M_{ER}}$ and as will be shown in section V, this threshold's value is higher than the femto prohibition zone of femtocells derived, hence will not violate outage constraint of edge femtocells if they employ co-channel operation from this point.

C. Femto Partitioning Threshold and Prohibition Zone Extension

As earlier stated, even though the minimum distance was derived for edge femtocells to safely reuse center macro resources, in this work we propose a new partitioning threshold for femtocells, R_f, such that $R_m \le R_f \le R_C$ as shown in Fig. 1(b), thereby extending the spectrum sharing prohibition zone for improved protection against severe cross-tier interference at the border region, commonly ignored in most prior works [4], [6]-[14]. Mathematically, we define the optimal R_f as;

$$R_f = r_{co-F_{\min}} + \frac{R_C - R_m}{2} \tag{29}$$

Since R_f is a function of $r_{co\text{-}F_{min}}$, it will also vary with all the key network parameters. In section V, the importance of the prohibition zone extension is elaborated by comparing three different scenarios for best throughput performance - (i) when femtocells utilize $r_{co\text{-}F_{min}}$ as center partitioning threshold, (ii) when femtocells utilize the same parameter with macrocell network, R_m, as CR threshold and lastly (iii) when R_f is used to partition the femtocell network into CR and ER respectively.

V. Performance Evaluation and Numerical Results

The analytical framework for UE SINR distribution is validated in this section via numerical simulation, and the effect of key network and system parameters on $r_{co\text{-}F_{min}}$ is clearly illustrated. We proceed further to analyze the use of R_f instead of R_m or $r_{co\text{-}F_{min}}$, as femto UE classifying parameter, and show the performance improvements as a result. The Numerical results obtained are from 5,000

Monte Carlo simulations. Main system parameters used are given in Table III for the downlink of a typical LTE/LTE-A network, while the macrocell antenna azimuth specifications are as defined in [12].

TABLE III: SIMULATION PARAMETERS

Parameters	Values		Parameters	Values
	Macro	Femto		
Topology	6-sectored, 19 Cells	PPP (in FBS/m^2) $\lambda_f = 0.00005 \sim 0.001$	Carrier Frequency	2 GHz
Coverage Radius	R_{HEX} =330m	R_{HeNB} =20m	System Bandwidth	20 MHz
Transmit Power	43 dBm	13 dBm	No. of RBs	100
Antenna Gain	$G_m^{(max)} = 18$ dBi	$G_F = 5$ dBi	sub-carrier spacing Δf	15 KHz
UE Gain, G_u	0 dBi	0 dBi	Shannon gap Φ	3 dB
No. of UEs	50 per MeNB	2 per HeNB	Rayleigh parameter μ	1

Parameters	Values	Parameters	Values
Outdoor path-loss exponent	4	Indoor path-loss exponent	3
Noise Density N_0	-174 dBm/Hz	Wall- loss ϑ	5~15 dB
Min. dist. between MeNB and UE	25m	No. of adaptive modulation Levels L	8
SINR Target Threshold γ	10 dB	Femto Outage Constraint ε_F	0.1

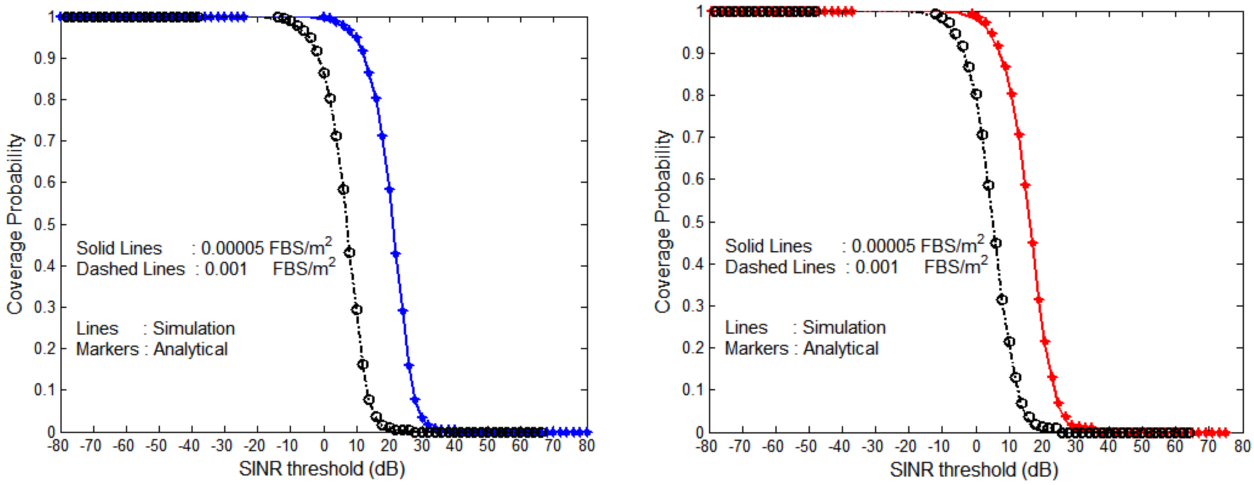

(a) Center region MUEs (b) Edge region MUEs

Fig. 2. Macro UEs coverage probability

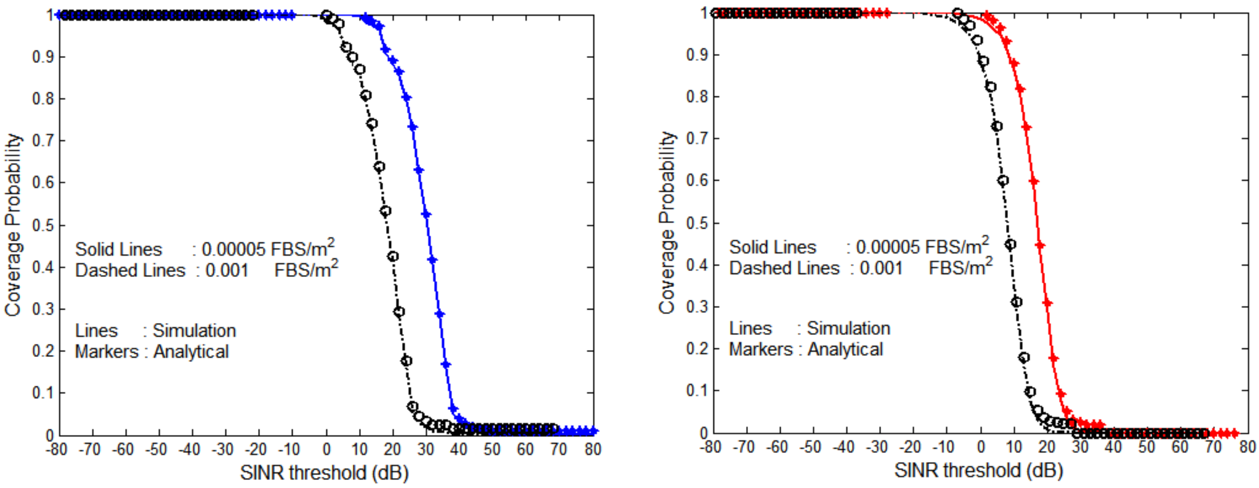

(a) Center region FUEs (b) Edge region FUEs

Fig. 3. Femto UEs coverage probability

The plots for all the derived UE coverage probabilities are given in Fig. 2 and Fig. 3 for varying femtocell densities where it is observed that results from the derived analytical expressions are in close agreement with those obtained from Monte Carlo simulations. This validates the analytical framework derived for the UE SINR distribution in this work. In all cases, it is evident that with increasing density of the closed-access femtocells, coverage performance for all UEs gets degraded due to rising interference, and can be easily observed from the expressions in (5), (20) - (22) where the coverage is a monotonically decreasing function of λ_f.

In Fig. 4, the minimum distance for edge femtocells to be able to reuse sub-band A (center macro spectrum) as derived in (24), is plotted against macrocell antenna azimuth for a 6 sector directional antenna. It shows that by using a 6-directional antenna, the peak values of $r_{co-F_{\min}} = 170$ m are observed at the bore-sight of the directional antenna of each macrocell sector $\Upsilon_1 = -60°$ $\Upsilon_2 = 0°, \Upsilon_3 = 60°, \Upsilon_4 = 120°, \Upsilon_5 = 180°$ and $\Upsilon_6 = 240°$, where cross-tier, macro-femto interference is highest, and reduces at the edges, implying that use of higher-sectored macrocell antennas allows for more co-channel femtocells to be deployed compared to omnidirectional antennas in line with [12] where a 3-sectored system was investigated.

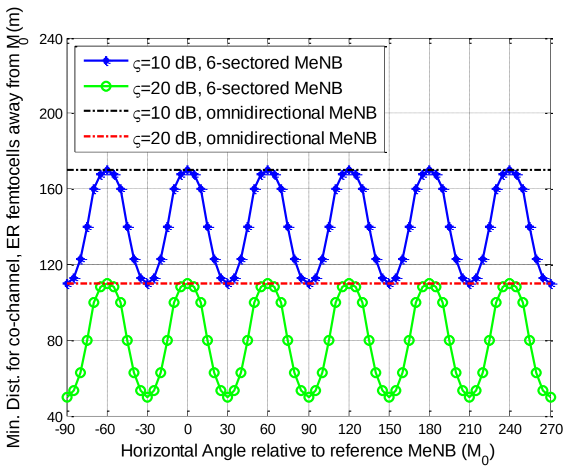

Fig 4. Spectrum sharing prohibition zone as a function of macrocell antenna azimuth with varying wall losses.

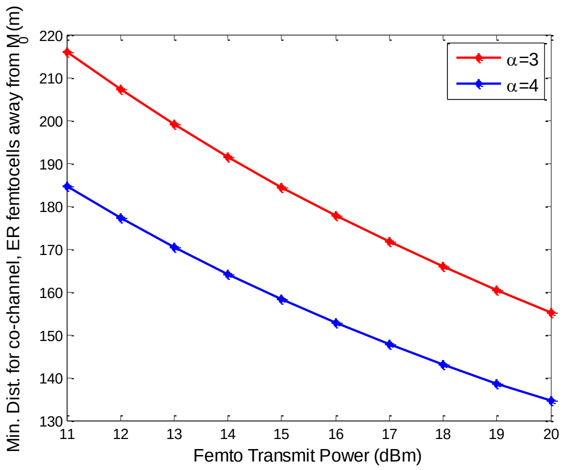

Fig. 5. Spectrum sharing zone as a function of femto transmit powers with varying path-loss exponents.

Also, higher wall-losses restrict the interfering signals penetration, thereby reducing the minimum distance for edge femtocells to share center macro spectral resources. Considering any fixed antenna azimuth where $r_{co-F_{\min}}$ is maximum (e.g. $\Upsilon_3 = 60°$), Fig. 5 is plotted to show the effect of varying femtocell transmit powers from 11 dBm to 20 dBm, on the co-channel minimum distance. Increasing P_f leads to decrease in $r_{co-F_{\min}}$ since the ability of FUEs to decode transmitted signals increases with increasing P_f, at a fixed P_M. However this would also lead to increase in cross-tier interference to nearby macro UEs, and hence femtocells should not transmit at the highest power always. Decreasing path-loss exponential value, α, corresponds to less attenuation of the electromagnetic waves and hence, increased impact of interfering signals, which leads to the increase in value of $r_{co-F_{\min}}$ as shown in Fig. 5, and also evident in (24) and (25). At $P_f = 13$ dBm and $\alpha = 4$, $r_{co-F_{\min}} \approx 170$ m is obtained as in Fig. 4 simulation.

In Fig. 6, the spatial threshold classifying MUEs into center and edge regions respectively, R_m is found as given in (28) when $T_{M_{CR}} = T_{M_{ER}}$ corresponding to a value of $R_m / R_C \approx 0.63$ or 190m away from M_0. As earlier stated, this guarantees some fairness level in resource distribution across both regions, because the center region would otherwise lead to high levels of R_m closer to 1, which even though could show high values for total macro throughput performance, would be at the detriment of degraded edge user throughput. Again, it is observed the close agreement between simulation and theoretical results.

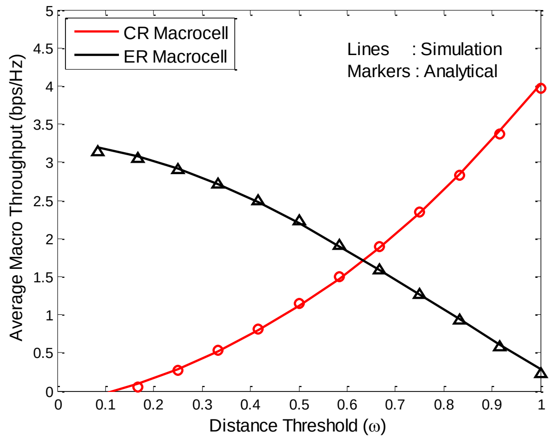

Fig. 6. Optimal macro spatial partition threshold, R_m, at $T_{M_{CR}} = T_{M_{ER}}$

Having obtained optimal values for $r_{co-F_{\min}}$ and R_m, we hereby derive the new femto partitioning threshold R_f as given in (29). In Fig. 7, some selected femtocells are studied in terms of spectrum usage with varying distances away from M_0.

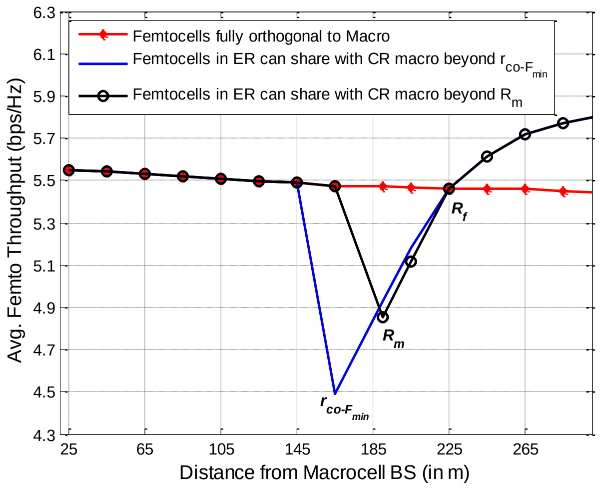

Fig. 7. Avg. femto throughput vs. distance away from MeNB, using different femto partitioning thresholds.

In Fig. 7, the first scenario is when the femtocells operate completely orthogonal to center macro UEs (do not use sub-band A), and have a steady throughput performance with slight reduction as the edge region is approached due to increasing cross-tier interference from neighbouring cells using the same edge sub-bands as corresponding femtocells. In the second case, $r_{co-F_{\min}}$ is used to partition FUEs into center and edge regions respectively, allowing ER femtocells to share same spectrum with center macro. This shows a severe dip in performance of boundary FUEs immediately upon reaching $r_{co-F_{\min}} \approx 170$ m due to intense interference from M_0, even though they would still have satisfied the outage constraint as defined for $r_{co-F_{\min}}$. Thirdly, when R_m is used, the observed dip is less than the $r_{co-F_{\min}}$ case since $R_m > r_{co-F_{\min}}$. Lastly, when R_f is employed, the femtocells performance seems to increase even further beyond this point, due to significant reduction in inter-tier interference with increased distance away from M_0, and also due to higher resources available to center region MUEs when FFR is employed. This shows that even though R_m and $r_{co-F_{\min}}$ could be used as in previous works to classify both macro and femto respectively, the use of R_f further reduces interference and allows femtocells to choose when best to opt for co-channel or orthogonal spectrum usage in such two-tier networks.

Fig. 8 goes further to investigate the FUE SINR performance under different schemes so as to directly observe the effects of the extended prohibition zone at boundary of center and edge regions. 10 randomly selected FUEs within the assumed boundary of cell-center and cell-edge are studied for the following cases:

1) This scheme employs full frequency reuse where both macro and femtocell tiers use same spectrum all the time. The poorest performance is observed for such FUEs due to severe cross-tier interference by the underlaying macrocells, especially M_0.
2) When $r_{co-F_{\min}}$ is used as the femto partitioning parameter, the quality of service constraints as discussed in section IV would be met, but the performance of boundary FUEs would not be optimal, especially at higher path-loss exponents where $r_{co-F_{\min}}$ would be reduced, thereby increasing likelihood of higher cross-tier interference from M_0.
3) Using R_m shows slightly better average performance for most of the FUEs due to increasing distance away from M_0, assuming other parameters and conditions remain unchanged
4) Lastly, by avoiding spectrum sharing within the extended prohibition zone, both FUEs and MUEs in this zone would benefit from reduced cross-tier interference, and possibly won't have to transmit with maximum power, leading to enhanced throughput and better efficiency. The reductions/gains in the FUE throughput performance values are seen not to be equally distributed all the time due to the irregular distribution of the femtocells within the boundary region.

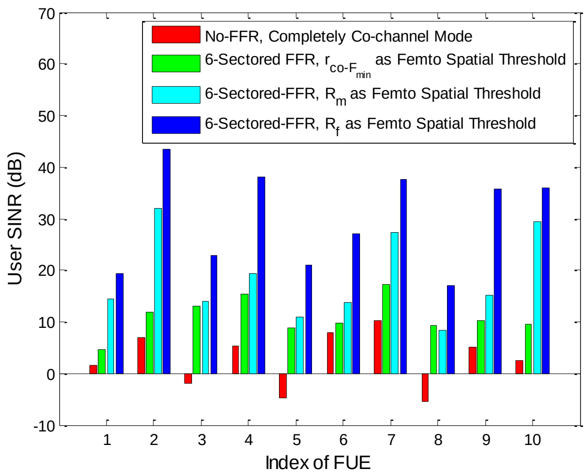

Fig. 8. Comparing FUE SINR performance at the boundary of CR and ER under different schemes.

VI. Conclusion

In this work, the deployment of femtocells under varying spectrum usage modes and spatial partitioning thresholds was studied using a combination of deterministic, hexagonal grid model for macro base station distribution, and a randomly distributed, set of closed-access femtocells based on the spatial PPP. Such a hybrid model allows for use of effective ICIC measures such as FFR, and utilization of six-sector antennas and at the same time enables the analytical derivation of important performance metrics such as coverage probability, throughput and the UE classification thresholds using tools of stochastic geometry. The UE coverage probability performance is seen to reduce with very dense femto deployments due to increasing interference, but the UEs still remain in coverage for reasonable SINR threshold values due to use of FFR and sectored antennas. Furthermore, the minimum distance for edge femtocells to be able to successfully share same spectrum with center macro UEs without violating the quality of service constraint is analytically and numerically derived, and its relation with key network parameters such as transmit power of femtocells and macrocell, path-loss exponent, wall-partition losses, pre-defined outage constraints and antenna azimuth is easily observed from (24) and also the simulation results. By using six-sectored antennas, it is found that more co-channel femtocells could be deployed around edges of the sectors where interference is less.

This work then compares the use of different spatial parameters for partitioning the macrocell and femtocell networks respectively, where it is observed that the proposed scheme employing the extended spectrum sharing prohibition zone was found to show superior throughput performance compared to other schemes commonly used in most prior works. Such arrangements provide system design guidelines in appropriate femtocell deployment and provisioning in multi-tier networks for improved interference reduction, efficient power utilization and hybrid spectrum usage.

REFERENCES

[1] D. L. Perez. X. Chu, Y. Yang, and F. Gunnarasson, *Heterogeneous Cellular Networks Theory, Simulation and Deployment*, New York, USA: Cambridge University press, 2013.

[2] P. Jacob, A. S. Madhukumar, and A. Alphones, “Interference mitigation through cross polarized transmission in femto-macro network,” *IEEE Communications Letters,* vol. 17, no. 10, pp. 1940-1943, 2013.

[3] V. Chandrasekhar and J. G. Andrews, “Spectrum allocation in tiered cellular networks,” *IEEE Transactions on Communications,* vol. 57, no. 10, pp. 3059-3068, 2009.

[4] I. Guvenc, J. Moo-Ryong, F. Watanabe, and H. Inamura, “A hybrid frequency assignment for femtocells and coverage area analysis for co-channel operation,” *IEEE Communications Letters,* vol. 12, no. 12, pp. 880-882, 2008.

[5] T. Zahir, K. Arshad, A. Nakata, and K. Moessner, “Interference management in femtocells,” *IEEE Communications Surveys & Tutorials*, vol. 15, no. 1, pp. 293-311, 2013.

[6] F. Wang and W. Wang, “Analytical evaluation of femtocell deployment in cellular networks using fractional frequency reuse,” *IET Communications*, vol. 8, no. 9, pp. 1599-1608, 2014.

[7] J. García-Morales, G. Femenias, and F. Riera-Palou, “Performance analysis and optimisation of FFR-aided OFDMA networks using channel-aware scheduling,” *Mobile Networks and Applications*, pp. 1-15, 2016.

[8] L. Liu, T. Peng, P. Zhu, Z. Qi, and W. Wang, “Analytical evaluation of throughput and coverage for FFR in OFDMA cellular network,” in *Proc. IEEE 83rd Vehicular Technology Conference (VTC Spring)*, Nanjing, 2016, pp. 1-5.

[9] H. Kalbkhani, V. Solouk, and M. G. Shayesteh, “Resource allocation in integrated femto-macrocell networks based on location awareness, “*IET Communications*, vol. 9, no. 7, pp. 917-932, 2015.

[10] A. S. Mohamed, M. Abd-Elnaby, and S. A. El-Dolil, “Self-organised dynamic resource allocation scheme using enhanced fractional frequency reuse in long term evolution-advanced relay-based networks,” *IET Communications*, vol. 10, no. 10, pp. 1163-1174, 2016.

[11] Y. Bai and L. Chen, “Hybrid spectrum arrangement and interference mitigation for co-existence between LTE macrocellular and femtocell networks,” *EURASIP Journal on Wireless Communications and Networking*, vol. 2013, no. 1, pp. 1-15, March 2013.

[12] J. Y. Wu, X. Chu, and D. L. Perez, “Downlink outage probability of co-channel femtocells in hierarchical 3-sector macrocells,” *IEEE Communication Letters*, vol. 16, no. 5, pp. 698-701, 2012.

[13] A. Mahmud and K. A. Hamdi, “On the co-channel femtocells exclusion region in fractional frequency reuse macrocells,” in *Proc. IEEE Wireless Communications and Networking Conference*, Istanbul, Turkey, 2014, pp. 2306-2311.

[14] C. Jia and T. J. Lim, “Designing femtocell exclusion zones to minimize power in a heterogeneous network,” in *Proc. IEEE Global Communications Conference*, Austin, TX, 2014, pp. 4251- 4256.

[15] S. Kumar, I. Z. Kovacs, G. Monghal, K. I. Pedersen, and P. E. Mogensen, “Performance evaluation of 6-sector-site deployment for downlink UTRAN long term evolution,” in *Proc. IEEE 68th Vehicular Technology Conference, (VTC Fall)*, Calgary, 2008, pp. 1-5.

[16] M. Haenggi, J. G. Andrews, F. Baccelli, O. Dousse, and M. Franceschetti, “Stochastic geometry and random graphs for the analysis and design of wireless networks,” *IEEE Journal on Selected Areas in Communications*, vol. 27, no. 7, pp. 1029-1046, 2009.

[17] R. W. Heath, M. Kountouris, and T. Bai, “Modelling heterogeneous network interference using poisson point processes,” *IEEE Transactions on Signal Processing*, vol. 61, no. 16, pp. 4114-4126, 2013.

[18] B. Blaszczyszyn and M. K. Karray, “Spatial distribution of the SINR in Poisson cellular networks with sector antennas,” *IEEE Transactions on Wireless Communications*, vol. 15, no. 1, pp. 581-593, 2016.

[19] M Haenggi, *Stochastic Geometry for Wireless Networks*, New York, USA: Cambridge University Press, 2013, pp. 101-111.

[20] I. S. Gradshtein, I. M. Ryzhik, and D. Zwillinger, *Tables of Integrals, Sums, Series, and Products*, 8^{th} ed., Massachusetts, USA: Academic Press, 2014, pp. 631-658.

Sani Umar Abdullahi received his B.Eng. degree in Electrical Engineering from Ahmadu Bello University Zaria, Nigeria in 2008 and an M.S. degree in Mobile and Satellite Communications from the Center for Communications and Systems Research (CCSR) of University of Surrey in 2009. He is currently pursuing a Ph.D. degree with the School of Communications and Computer Engineering, University of Science and Technology (USTB), Beijing, China. His research interests include; Heterogeneous Networks, Millimeter wave Communications, Hybrid (Satellite-Terrestrial Systems), Interference Management and Resource Allocation.

Jian Liu received his B.S. degree in Automatic Control Theory and Applications from Shandong University, China, in 2000, and the Ph.D. degree in School of Information Science and Engineering from Shandong University in 2008. He is currently an associate professor of University of Science and Technology (USTB), Beijing, China. His research interests include cognitive radio networks, mobile mesh networks, and LTE-A.

Seyed Alireza Mohadeskasaei received his BS and MS degrees in Electronics Engineering from the School of Electronic Engineering, Islamic Azad University, Najafabad branch, Iran in 2003 and 2005 respectively. He is currently pursuing a PhD degree with School of Communications and Computer Engineering, University of Science and Technology (USTB), Beijing, China. His research interests include; modeling and simulation of RF systems, wide band power amplifiers, millimeter wave networks and energy efficiency in mobile and ad-hoc networks.